The physics of ultrafast saturable absorption in graphene

Xing, Guichuan; Guo, Hencheng; Zhang, Xinhai; Sum, Tze Chien; Huan, Alfred Cheng Hon

2010

Xing, G., Guo, H., Zhang, X., Sum, T. C., & Huan, A. C. H. (2010). The physics of ultrafast saturable absorption in graphene. Optics express, 18(5), 4564-4573.

https://hdl.handle.net/10356/79994

https://doi.org/10.1364/OE.18.004564

The Physics of ultrafast saturable absorption in graphene

Guichuan Xing,[1] Hongchen Guo,[2] Xinhai Zhang,[2] Tze Chien Sum,[1]* and Cheng Hon Alfred Huan[1]

[1]*Division of Physics and Applied Physics, School of Physical and Mathematical Sciences, Nanyang Technological University,21 Nanyang Link, 637371, Singapore*

[2]*Institute of Materials Research and Engineering, A* STAR (Agency for Science, Technology and Research), 3 Research Link, 117602, Singapore*

**tzechien@ntu.edu.sg*

Abstract: The ultrafast saturable absorption in graphene is experimentally and theoretically investigated in the femtosecond (fs) time regime. This phenomenon is well-modeled with valence band depletion, conduction band filling and ultrafast intraband carrier thermalization. The latter is dominated by intraband carrier-carrier scattering with a scattering time of 8 (± 3) fs, which is far beyond the time resolution of other ultrafast techniques with hundred fs laser pulses. Our results strongly suggest that graphene is an excellent atomic layer saturable absorber.

OCIS codes: (160.4236) Nanomaterials; (190.4400) Nonlinear Optics, Materials; (320.7110) Ultrafast nonlinear optics

References and links

1. P. R. Wallace, "The band theory of graphite," Phys. Rev. **71**(9), 622–634 (1947).
2. A. H. Castro Neto, F. Guinea, N. M. R. Peres, K. S. Novoselov, and A. K. Geim, "The electronic properties of graphene," Rev. Mod. Phys. **81**(1), 109–162 (2009).
3. A. K. Geim, and K. S. Novoselov, "The rise of graphene," Nat. Mater. **6**(3), 183–191 (2007).
4. P. Avouris, Z. Chen, and V. Perebeinos, "Carbon-based electronics," Nat. Nanotechnol. **2**(10), 605–615 (2007).
5. T. Ando, Y. S. Zheng, and H. Suzuura, "Dynamical Conductivity and Zero-Mode Anomaly in Honeycomb Lattices," J. Phys. Soc. Jpn. **71**(5), 1318–1324 (2002).
6. V. P. Gusynin, S. G. Sharapov, and J. P. Carbotte, "Unusual microwave response of dirac quasiparticles in graphene," Phys. Rev. Lett. **96**(25), 256802 (2006).
7. T. Stauber, N. M. R. Peres, and A. K. Geim, "Optical conductivity of graphene in the visible region of the spectrum," Phys. Rev. B **78**(8), 085432 (2008).
8. A. B. Kuzmenko, E. van Heumen, F. Carbone, and D. van der Marel, "Universal optical conductance of graphite," Phys. Rev. Lett. **100**(11), 117401 (2008).
9. F. Wang, Y. Zhang, C. Tian, C. Girit, A. Zettl, M. Crommie, and Y. R. Shen, "Gate-variable optical transitions in graphene," Science **320**(5873), 206–209 (2008).
10. R. R. Nair, P. Blake, A. N. Grigorenko, K. S. Novoselov, T. J. Booth, T. Stauber, N. M. R. Peres, and A. K. Geim, "Fine structure constant defines visual transparency of graphene," Science **320**(5881), 1308 (2008).
11. K. F. Mak, M. Y. Sfeir, Y. Wu, C. H. Lui, J. A. Misewich, and T. F. Heinz, "Measurement of the optical conductivity of graphene," Phys. Rev. Lett. **101**(19), 196405 (2008).
12. J. M. Dawlaty, S. Shivaraman, M. Chandrashekhar, F. Rana, and M. G. Spencer, "Measurement of ultrafast carrier dynamics in epitaxial graphene," Appl. Phys. Lett. **92**(4), 042116 (2008).
13. D. Sun, Z. K. Wu, C. Divin, X. Li, C. Berger, W. A. de Heer, P. N. First, and T. B. Norris, "Ultrafast relaxation of excited Dirac fermions in epitaxial graphene using optical differential transmission spectroscopy," Phys. Rev. Lett. **101**(15), 157402 (2008).
14. R. W. Newson, J. Dean, B. Schmidt, and H. M. van Driel, "Ultrafast carrier kinetics in exfoliated graphene and thin graphite films," Opt. Express **17**(4), 2326–2333 (2009).
15. M. Breusing, C. Ropers, and T. Elsaesser, "Ultrafast carrier dynamics in graphite," Phys. Rev. Lett. **102**(8), 086809 (2009).
16. J. Wang, Y. Hernandez, M. Lotya, J. N. Coleman, and W. J. Blau, "Broadband Nonlinear Optical Response of Graphene Dispersions," Adv. Mater. **21**(23), 2430–2435 (2009).
17. Z. Liu, Y. Wang, X. Zhang, Y. Xu, Y. Chen, and J. Tian, "Nonlinear optical properties of graphene oxide in nanosecond and picosecond regimes," Appl. Phys. Lett. **94**(2), 021902 (2009).
18. A. C. Ferrari, J. C. Meyer, V. Scardaci, C. Casiraghi, M. Lazzeri, F. Mauri, S. Piscanec, D. Jiang, K. S. Novoselov, S. Roth, and A. K. Geim, "Raman spectrum of graphene and graphene layers," Phys. Rev. Lett. **97**(18), 187401 (2006).

#122085 - $15.00 USD Received 4 Jan 2010; revised 9 Feb 2010; accepted 9 Feb 2010; published 19 Feb 2010

19. Z. H. Ni, W. Chen, X. F. Fan, J. L. Kuo, T. Yu, A. T. S. Wee, and Z. X. Shen, "Raman spectroscopy of epitaxial graphene on a SiC substrate," Phys. Rev. B **77**(11), 115416 (2008).
20. J. C. Burton, L. Sun, F. H. Long, Z. C. Feng, and I. T. Ferguson, "First- and second-order Raman scattering from semi-insulating 4H-SiC," Phys. Rev. B **59**(11), 7282–7284 (1999).
21. D. Graf, F. Molitor, K. Ensslin, C. Stampfer, A. Jungen, C. Hierold, and L. Wirtz, "Spatially resolved Raman spectroscopy of single- and few-layer graphene," Nano Lett. **7**(2), 238–242 (2007).
22. J. Hass, F. Varchon, J. E. Millán-Otoya, M. Sprinkle, N. Sharma, W. A. de Heer, C. Berger, P. N. First, L. Magaud, and E. H. Conrad, "Why multilayer graphene on 4H-SiC(0001[over]) behaves like a single sheet of graphene," Phys. Rev. Lett. **100**(12), 125504 (2008).
23. M. Sheik-Bahae, A. A. Said, T. H. Wei, D. J. Hagan, and E. W. Van Stryland, "Sensitive measurement of optical nonlinearities using a single beam," IEEE J. Quantum Electron. **26**(4), 760–769 (1990).
24. Y. R. Shen, "The Principles of Nonlinear Optics," John Wiley, New York and Chichester, **1984**, pp. 334–336, 437–446.

1. Introduction

Graphene is new class of single atom thick materials which possesses a unique smooth-sided conical band structure that converges to a single Dirac point [1–4]. In the recent years, graphene has been subjected to extensive studies [1–19]. Among these studies, there are several reports on the effects of weak light interaction with graphene. Within the model of the non-interacting, massless Dirac fermions [1,2], the weak light absorption is calculated to be independent of frequency and to have a universal opacity, $\pi \cdot \alpha = 2.3\%$ (where α is the fine structure constant) [5–7]. This theoretical prediction has been confirmed by recent infrared to visible reflectivity and transmission measurements [8–11]. However, studies on the coupling between photons and fermions in graphene under high intensity, ultrashort laser pulse excitation are limited [12–17]. In particular, the relationship between the nonlinear optical properties of graphene and the basic fine structure constant has never been investigated.

Here, we experimentally characterized and theoretically modeled the ultrafast saturable absorption in graphene, which was epitaxially grown on a transparent wide bandgap semiconductor SiC substrate. Our findings revealed that graphene possesses excellent saturable absorption properties with low saturation intensity; controllable saturation depth; ultrafast recovery time; near symmetric spatio-temporal narrowing and high damage threshold. Its ultrafast saturation absorption properties are well-described by the effects of valence band depletion, conduction band filling and ultrafast intraband carrier relaxation. The latter is dominated by intraband carrier-carrier (c-c) scattering with a scattering time of 8 (± 3) femtoseconds (fs), which is far beyond the time resolution of other ultrafast techniques with hundred fs laser pulses. Graphene presents us with a unique system to model these non-linear effects with fundamental physics. Key to the development of practical graphene-based optoelectronic devices is through a clear understanding of its intrinsic optical properties.

2. Graphene characterization

In our experiments, bi-layer graphene with rotational stacking faults (30.0 or ± 2.20°) was epitaxially grown on both sides of a 0.4 mm thick n-type C-terminated 6H-SiC (0001) substrate. The thickness of graphene was measured by monitoring the attenuation of the bulk SiC component in the Si 2p photoemission spectroscopy signal and confirmed with the Raman spectrum [18–21]. Due to the different stacking structure compared to hexagonal Bernal graphite, the layers are effectively decoupled [22]. Raman spectroscopy was performed to determine the quality of the epitaxial graphene as well as to confirm the number of layers. The measurements were carried out with a WITEC CRM200 Raman system with 488 nm (2.54 eV) excitation and a spot size of diameter ~500 nm with a 100 × microscope objective (NA = 0.95).

In Fig. 1, the in-plane vibrational G peak at ~1577 cm^{-1} and the two-phonon 2D peak at ~2717 cm^{-1} are clearly identifiable. The smaller peaks at ~1520 cm^{-1} and ~1713 cm^{-1} originate from the 4H-SiC substrate. The former is the overtone of the SiC TO(X) phonon at 761 cm^{-1} while the latter is a combination of the optical phonons with wave vectors near the M point at the zone edge of the SiC substrate [19,20]. The relatively small defect-induced D band (~1360 cm^{-1}) suggests good crystallinity in the graphene samples. The comparable

#122085 - $15.00 USD Received 4 Jan 2010; revised 9 Feb 2010; accepted 9 Feb 2010; published 19 Feb 2010

Raman intensity of the G band and the 2D band as well as the broad 2D band (at 100 cm^{-1}) confirms the primarily two-layer nature of the graphene sample [19]. A Raman image obtained using the intensity of the G-band is shown in the inset of Fig. 1. The G-band intensity is known to increase almost linearly with the number of graphene layers [21]. The relative uniformity of the graphene layers is also evident from the large area uniformity of the G-band intensity shown in Fig. 1 inset.

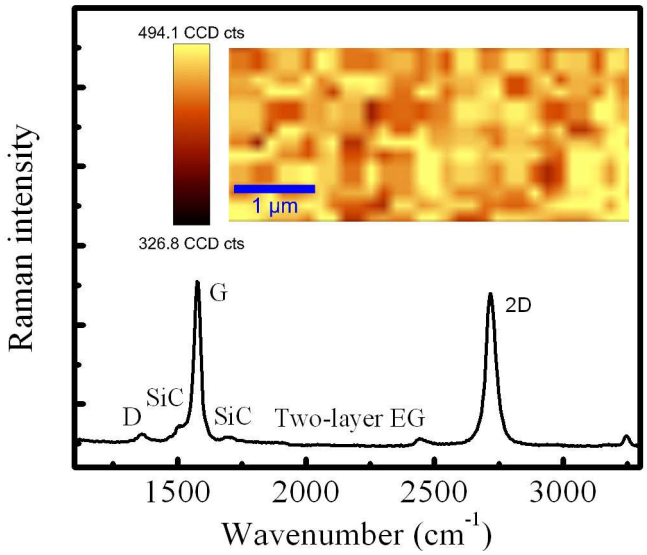

Fig. 1. Representative Raman spectrum of two-layer epitaxial graphene (EG) on SiC. The inset is Raman image of the intensity of the G-band. Scale bar = 1 um.

3. Ultrafast saturable absorption investigation

Z-scan technique was used to investigate the pump intensity dependent transmittance [23]. The 1 kHz, 200fs wide laser pulses, centered at 800 nm, were generated from a Coherent Legend™ regenerative amplifier that was seeded by a Coherent Mira™ oscillator. The full-width-at-half-maximum of the photon energy dispersion was 0.04 eV. The laser pulse was focused perpendicular on the sample with a lens of focal length 30 cm. The beam waist at the focus was 31 ± 2 μm and was confirmed with a standard two-photon absorption experiment on a 0.5 mm thick ZnSe bulk crystal. In our experiments, as the graphene sample was translated through the focal point along the laser propagation axis, the transmittances at different z positions were recorded. The effects of the ultrafast saturable absorption and the spatio-temporal reshaping of the transmitted 800nm fs pulses in graphene were analyzed. The response from a bare SiC substrate was also measured under the same conditions and at the same pump intensities (≤ 120 GW/cm^2) where negligible nonlinear absorption has been found. The nonlinear absorption from SiC substrate will be obvious at 200 GW/cm^2, where, graphene still shows saturable absorption.

#122085 - $15.00 USD Received 4 Jan 2010; revised 9 Feb 2010; accepted 9 Feb 2010; published 19 Feb 2010

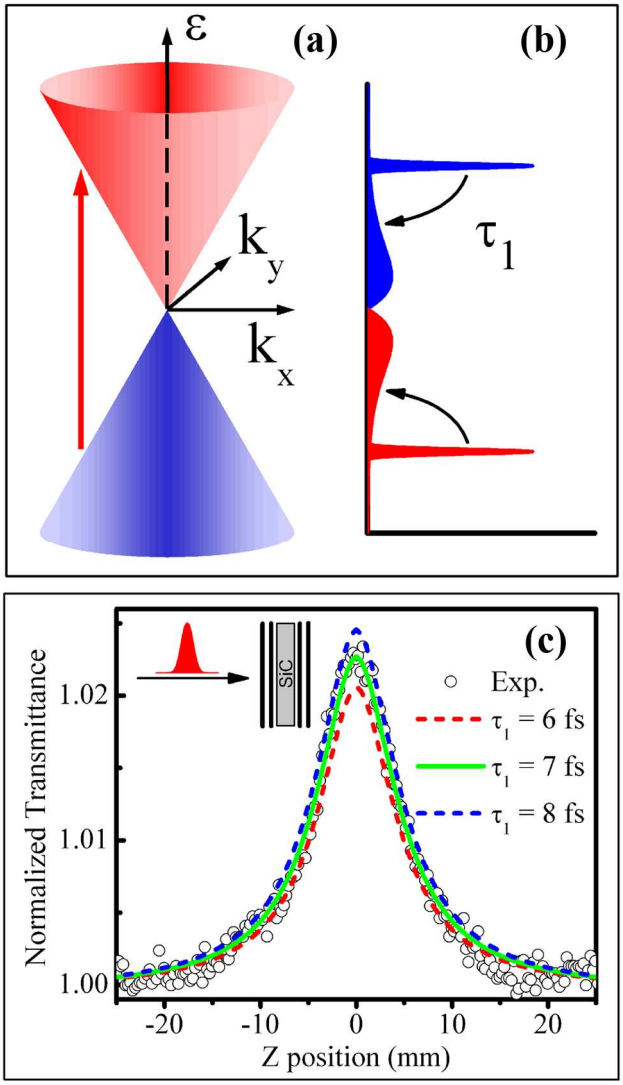

Fig. 2. (a) The momentum conserved photon absorption process in graphene (b) Instantaneous photon absorption generate nonequilibrium distributions of electrons (**blue**) and holes (**red**), which subsequently thermalize through ultrafast intraband carrier-carrier and carrier-optical phonon scattering to form Fermi-Dirac distributions (c) Typical nonlinear transmittance of graphene layers at different Z position (circle dots) and the theoretical predictions with Eq. (11) using different τ_1. The inset shows a schematic of the Gaussian laser pulse transmission through the graphene layers.

In graphene, the excitation process near the Dirac point can be described by the Dirac Hamiltonian with linear wavevector dependent energy dispersion ($\varepsilon = \hbar v_F|k|$, where $v_F = 10^6$ *m/s* is the Fermi velocity) as shown in Fig. 2(a). For epitaxially grown graphene layers on SiC substrate, the first layer is highly doped and the Fermi level is located at approximately 0.35 eV in conduction band [13]. However, this doping will not affect the photon absorption at 1.55 eV [Fig. 1(a)]. After photoexcitation by 1.55 eV (800 nm) fs laser pulses, a non-equilibrium population of electrons in the conduction band ($\varepsilon = \hbar\omega/2$) and holes in valence band ($\varepsilon = -\hbar\omega/2$) is created with momentum conservation. Here, the effects of triangular warping and other nonlinear effects have been found to be negligible even at visible

#122085 - $15.00 USD Received 4 Jan 2010; revised 9 Feb 2010; accepted 9 Feb 2010; published 19 Feb 2010

wavelengths (i.e. up to 3.1 eV) [7,10]. From Fermi's golden rule, the instantaneous absorbed power is:

$$W_t^a = \frac{2\pi}{\hbar}\cdot\left|M_t\right|^2 \cdot D(\frac{\hbar\omega}{2})\cdot[f_t(-\frac{\hbar\omega}{2}) - f_t(\frac{\hbar\omega}{2})]\cdot\hbar\omega \quad (1)$$

where $\hbar\omega$ is the photon energy, $D(\pm\hbar\omega/2) = \hbar\omega/(\pi\hbar^2 v_F^2)$ are the density of states at $\varepsilon = \pm\hbar\omega/2$ and $f_t(\varepsilon)$ is the electron occupation probability at time t. The Dirac fermion transition matrix M_t from initial state $|m\rangle$ to final state $|n\rangle$ under the perturbation of incident electromagnetic field at time t is [10]:

$$\left|M_t\right|^2 = \left|\left\langle n\left| v_F\cdot\vec{\sigma}\cdot\frac{e}{i\omega}\vec{E}_t\right|m\right\rangle\right|^2 = \frac{1}{8}e^2 v_F^2\frac{I_t}{\omega^2} \quad (2)$$

where $\vec{E}_t$ is the electric field component, $I_t = \left|E_t\right|^2$ and $\vec{\sigma}$: are the standard Pauli matrices.

Under low optical excitation where the carriers undergo fast interband decay in graphene [12–15], it is reasonable to use the following approximations: $f_t(-\hbar\omega/2) \approx 1$ and $f_t(\hbar\omega/2) \approx 0$. With the incident power $W_t^i = (c/4\pi)I_t$, the linear optical transmittance can be calculated as:

$$T[t] = 1 - \frac{W_t^a}{W_t^i} = 1 - \pi\frac{e^2}{\hbar c} = 1 - \pi\alpha \quad (3)$$

It is dependent on the fine structure constant α but independent of the excitation wavelength and the material parameter v_F.

In contrast, high intensity excitation creates large temporal populations of carriers in the valence band (VB) and the conduction band (CB). Further absorption of incoming photons at the same energy (within the pulse duration) will be reduced, giving rise to a bleaching effect seen in Fig. 2(c) as increased transmittance. Concurrently, the nonequilibrium carrier distributions in the CB and VB will undergo ultrafast intraband relaxation through non-dissipative c-c scattering and to a slower extent by carrier-optical phonon (c-op) coupling. Free carrier absorption in graphene is unlikely as such process require the assistance of phonons for momentum conservation. Thermalization is quickly achieved leaving ultra high temperature Fermi-Dirac distributions in the VB and CB [Fig. 2(b)]. Subsequently, optical and acoustic phonon processes take place on a longer timescale to cool the carrier distributions along with electron-hole recombination [12–15]. For a Gaussian temporal pump pulse with uniform spatial component, I_t can be expressed as $I_0 \exp(-t^2/\tau^2)$. The dynamics for VB and CB electron occupation probabilities $f(\mp\varepsilon)$ can then be described by:

$$\frac{\partial f(-\varepsilon)}{\partial t} = -f(-\varepsilon)\cdot\frac{\pi\alpha}{D(\varepsilon)}\frac{I_0}{\hbar w}\cdot\exp[-\frac{t^2}{\tau^2}] + f(\varepsilon)\cdot\frac{\pi\alpha}{D(\varepsilon)}\frac{I_0}{\hbar w}\cdot\exp[-\frac{t^2}{\tau^2}] + \frac{1-f(-\varepsilon)}{\tau_1} \quad (4)$$

$$\frac{\partial f(\varepsilon)}{\partial t} = -f(\varepsilon)\cdot\frac{\pi\alpha}{D(\varepsilon)}\frac{I_0}{\hbar w}\cdot\exp[-\frac{t^2}{\tau^2}] + f(-\varepsilon)\cdot\frac{\pi\alpha}{D(\varepsilon)}\frac{I_0}{\hbar w}\cdot\exp[-\frac{t^2}{\tau^2}] - \frac{f(\varepsilon)}{\tau_1} \quad (5)$$

Where τ is half-width at $1/e$ of the maximum of laser pulse and τ_1 is the ultrafast carrier relaxation time which is dominated by intraband c-c scattering. The first and second terms on the right hand side (RHS) of Eqs. (4) and (5) represent the photon-absorption-induced electron occupation probability balance between the valence band and conduction band. The third term on the RHS of Eq. (4) (or Eq. (5)) is derived from hole (or electron) relaxation increasing (or decreasing) in the valence (or conduction) band respectively. The initial conditions prior to laser excitation are:

#122085 - $15.00 USD Received 4 Jan 2010; revised 9 Feb 2010; accepted 9 Feb 2010; published 19 Feb 2010

$$f_{-\infty}(-\hbar\omega/2)=1;\quad f_{-\infty}(\hbar\omega/2)=0; \tag{6}$$

Equations (4), (5) and (6) can be solved together to give the result as:

$$f_t(-\hbar\omega/2)-f_t(\hbar\omega/2)=1-2\frac{\pi\alpha I_0}{D(\hbar\omega/2)\cdot\hbar\omega}\cdot G(t) \tag{7}$$

where

$$G(t)=\int_{-\infty}^{t}\exp[-\frac{x^2}{\tau^2}+\frac{x-t}{\tau_1}+\frac{\pi\alpha I_0}{D(\hbar\omega/2)\cdot\hbar\omega}\cdot\sqrt{\pi}\cdot\tau\cdot(Erf[\frac{x}{\tau}]-Erf[\frac{t}{\tau}])]\cdot dx \tag{8}$$

and $Erf[x]$ is the Gaussian error function.

The absorbed energy per unit area for one pulse can be written as:

$$Abs[I_0]=\int_{-\infty}^{\infty}(f_t(-\hbar\omega/2)-f_t(\hbar\omega/2))\cdot\pi\alpha I_0\cdot\exp[-\frac{t^2}{\tau^2}]\cdot dt \tag{9}$$

For a real focused Gaussian laser pulse, both the temporal and spatial profiles follow a Gaussian distribution, then

$$I_0=I_{00}\cdot\exp[-\frac{2r^2}{w^2}]\cdot(1+\frac{z^2}{z_0^2})^{-1} \tag{10}$$

where $z_0=\pi w_0^2/\lambda$ is the diffraction length, $w=w_0\cdot[1+(z/z_0)^2]^{1/2}$ is the beam waist, w_0 is the minimum beam waist, λ is the pump laser wavelength, z is on-axis relative position to the focal point, r is radial coordinate and I_{00} is the on-axis peak irradiance at the focal point.

Integrating Eq. (9) over the cross-section at z, the absorbed energy per pulse is:

$$W^a=\int_0^{\infty}Abs[I_{00}\cdot\exp[-\frac{2r^2}{w^2}]\cdot(1+\frac{z^2}{z_0^2})^{-1}]\cdot 2\pi r\cdot dr \tag{11}$$

Using Eq. (11), a good fit of the experimental data in Fig. 2(c) (solid line) is obtained with τ_1 as the only fitting parameter. Our fitted value τ_1 (7 ± 3 fs) agrees well with the 13 ± 3 fs intraband carrier equilibration time reported by Breusing *et al*. for 20 – 30 nm thick graphite that was probed using transient absorption spectroscopy with 7 fs laser pulses [15]. τ_1 comprises contributions from both the intraband c-c scattering and the dissipative c-op coupling, i.e. $\tau_1=\tau_{c\text{-}c}\,\tau_{c\text{-}op}/(\tau_{c\text{-}c}+\tau_{c\text{-}op})$, where $\tau_{c\text{-}c}$ and $\tau_{c\text{-op}}$ refer to the lifetimes for c-c scattering and c-op coupling respectively. It is usual that $\tau_{c\text{-op}}\gg\tau_{c\text{-}c}$ so that $\tau_1\approx\tau_{c\text{-}c}$. A typical value of $\tau_{c\text{-}op}$ is ~100 fs [15]. From this approximation, the ultrafast intraband c-c scattering time, $\tau_{c\text{-}c}$ is calculated to be 8 ± 3 fs. Such ultrafast dynamics in graphene is far beyond the temporal resolution of typical pump-probe experiments conducted with hundred fs pulses [12,14].

Next, we consider the ultrafast intraband carrier thermalization (dominated by the intraband c-c scattering) in the absence of energy dissipation. Transient Fermi-Dirac distributions can be established at ultra high temperatures T_0 with different chemical potentials (μ_e and μ_h) according to the following conditions of particle number and energy conservation:

$$n=\int_0^{\infty}D(\varepsilon)f_{FD}(\varepsilon)d\varepsilon\quad\text{and}\quad\frac{1}{2}n\hbar\omega=\int_0^{\infty}\varepsilon D(\varepsilon)f_{FD}(\varepsilon)d\varepsilon \tag{12}$$

where $f_{FD}(\varepsilon)=(1+\exp((\varepsilon-\mu)/k_BT_e))^{-1}$.

#122085 - $15.00 USD Received 4 Jan 2010; revised 9 Feb 2010; accepted 9 Feb 2010; published 19 Feb 2010

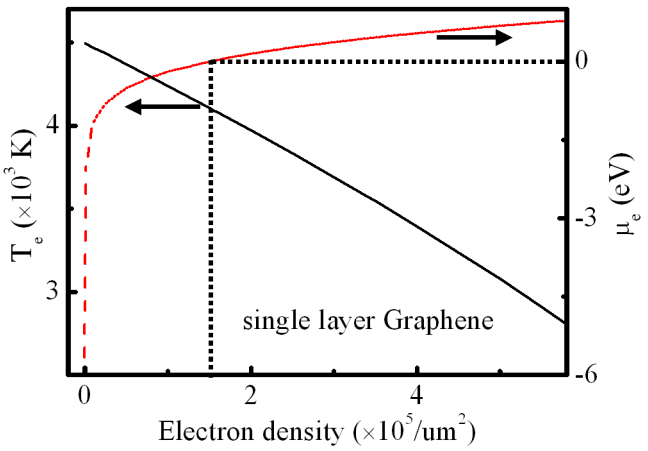

Fig. 3. Thermalized electron temperature (T_e) and the corresponding chemical potential (μ_e) as a function of electron density, excited at 1.55 eV.

When exciting a single layer of graphene with $\hbar\omega$ = 1.55 eV photons, the dependence of the electron temperature (T_e) and corresponding chemical potential (μ_e) on the electron density (N_e) are shown in Fig. 3. The thermalized T_e mono decreases while the corresponding μ_e mono increases as N_e increases. For $N_e = 1.9 \times 10^5/\text{um}^2$, a thermalized T_e = 4000 K will be obtained. At the threshold electron density, $N_{th} = 1.5 \times 10^5/\text{um}^2$, the thermalized temperature is equal to the Fermi temperature of N_{th}. This corresponds to $\mu_e(N_{th}) = 0$. For electron density $N_e < N_{th}$ (in the limit of low laser pump intensity), the established temperature will be greater than the Fermi temperature of N_e. At this electron density, more of the fermions are in the higher excited states within the CB. This results in $\mu_e(N_e) < 0$. One possibility is that at high temperatures, the fermion gas approaches the classical ideal gas. In addition, the threshold electron density N_{th} is dependent on the pump photon energy ($\hbar\omega$). With $\mu_e = 0$ and the conditions of Eq. (12), the following relationship can be deduced: $N_{th} = 8.9\times10^{-5}\pi^5(\hbar\omega)^2/(\hbar v_F)^2$. In the absence of optical phonon coupling, under 1.55 eV photon excitation, the highest electron density that can be populated in graphene is around 5.8 $\times 10^5/\text{um}^2$. Beyond this upper limit, 100% transmittance for the subsequent incoming photons will be observed.

The effects of sudden photon absorption and subsequent c-c scattering on the intrinsic ultrafast saturable absorption of monolayer graphene can be demonstrated from the temporal and spatial distortion in the transmitted laser pulses. From Eq. (7), the temporal transmittance at t is derived as:

$$T(t) = 1 - \pi\alpha + \frac{2I_0}{D(\hbar\omega/2)\cdot\hbar\omega}\cdot G(t)\cdot(\pi\alpha)^2 \tag{13}$$

Likewise, the transverse transmittance at $z = 0$ can be written as:

$$T(r) = 1 - \frac{Abs[I_{00}\cdot\exp(-2r^2/w_0^2)]}{I_{00}\tau\sqrt{\pi}\cdot\exp(-2r^2/w_0^2)} \tag{14}$$

From these, the transmitted temporal and spatial profiles through graphene are calculated for different intensities and plotted in Fig. 4(b) and 4(d). The solid lines in Fig. 4(b) are derived from τ_1 = 7 fs along with the same parameters as used in our experiments. Similarly, the calculated spatial profiles are shown in Fig. 4(d). For comparison, the input temporal and spatial laser profiles are plotted in Fig. 4(a) and 4(c). In Fig. 4(b) the calculated maximum transmittance occur a few fs after time zero which is taken to be the center of the temporal profile. This asymmetry in the temporal profile arises due to the two competing processes

#122085 - $15.00 USD Received 4 Jan 2010; revised 9 Feb 2010; accepted 9 Feb 2010; published 19 Feb 2010

during the accumulation of carriers in the VB and CB: photo absorption of incoming photons at the same energy (within the pulse duration) and the intraband c-c scattering (that leads to the redistribution of the carriers). This causes a delay in reaching the maximum transmittance. The narrowing of the temporal profile of the transmitted pulses occurs when the pump intensity is increased from 1 to 5 GW/cm^2. But this effect becomes less obvious at higher pump intensities (80 GW/cm^2). This is attributed to the saturation of the saturable absorption, which is dependent on the saturation depth of the materials. From Fig. 4(d), the narrowing of the spatial profiles shows a similar trend to that of the temporal profiles. Unlike the temporal case, the transmittances of the spatial profile always show symmetrical narrowing.

The transmitted laser pulse temporal shape is strongly dependent on the intraband carrier thermalization time. To clearly illustrate this dependence, the dashed lines in Fig. 4(b) were calculated using τ_1 = 100 fs and all other parameters remain the same. The narrowing of the temporal profile and the subsequent saturation of the saturable absorption occurs at much lower pump intensities compared to that with τ_1 = 7 fs. In light of the competing processes discussed earlier, the temporal transmittance profile is more asymmetrical. The transmittance also has a longer tail, which is caused by the slower intraband carrier relaxation.

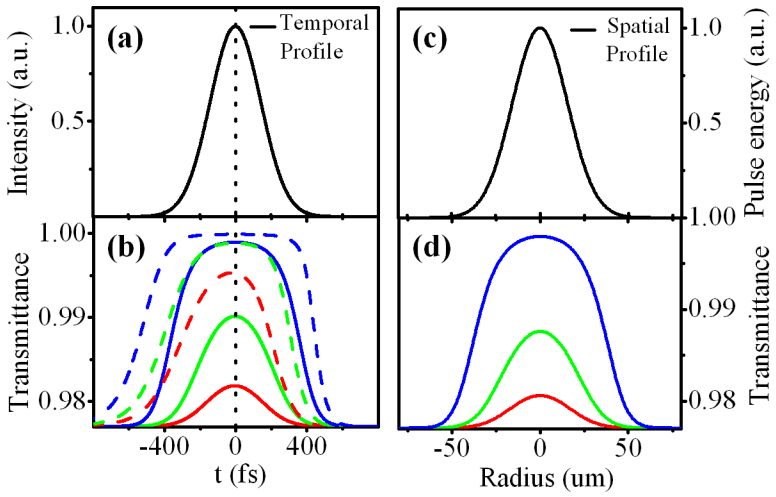

Fig. 4. Input laser pulse (a) temporal (c) spatial profile, Gaussian laser pulse (b) temporal transmittances with τ_1 = 7 fs (solid lines) and τ_1 = 100 fs (dashed lines), (d) spatial transmittances with τ_1 = 7 fs at peak pump intensity of 1 GW/cm^2 (**red**), 5 GW/cm^2 (**green**) and 80 GW/cm^2 (**blue**).

The strong saturable absorption in atomic layer graphene is attributed to two main reasons: Firstly, the wavelength independent strong linear absorption ($\pi\alpha$ = 2.3%) of graphene provides a potential saturable absorption depth (i.e. maximum change in transmittance). This large linear absorption arises from the unique properties of graphene: i.e. two dimensional massless fermions and a conical band structure. Secondly, the excited states absorption in graphene is momentum forbidden and they require the assistance of phonons. The only photon coupling process for the excited state electrons is through stimulated emission ($\varepsilon(\hbar\omega/2) \rightarrow \varepsilon(-\hbar\omega/2)$). The nonlinear optical properties of graphene and graphene oxide were previously investigated using picosecond and nanosecond lasers on small pieces of sample dispersed in a solution [16,17]. However, the high thermal conductivity, large linear absorption and small sample size together with the long laser pulses will inevitably generate solvent bubbles and micro-plasmas. In contrast to our findings, these earlier results were dominated by the nonlinear scattering.

#122085 - $15.00 USD Received 4 Jan 2010; revised 9 Feb 2010; accepted 9 Feb 2010; published 19 Feb 2010

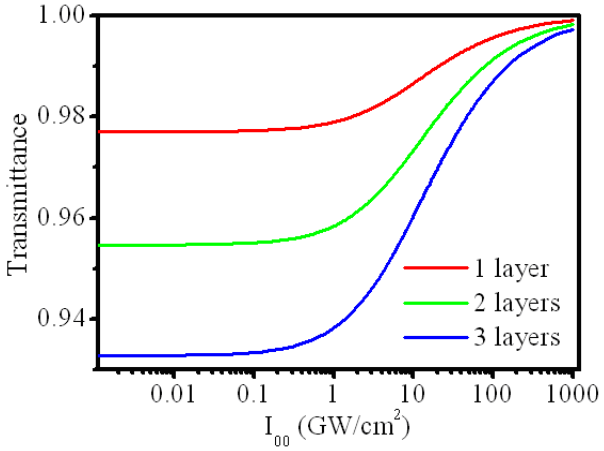

Fig. 5. Transmittance vs. incident pump intensity for different layers of graphene.

It is also possible to control the saturation depth in graphene through varying the number of atomic layers. As the epitaxial grown layers on SiC are effectively decoupled, the light can be considered to be transmitting sequentially through different layers. Figure 5 shows the calculated transmission dependence on the incident pump intensity for different atomic layers at the focal point. It clearly shows that the saturation depth is nearly proportional to the number of layers and the saturation onset is as low as 0.1 GW/cm^2. However, due to the ultrafast intraband c-c dynamics, a pump intensity as high as 1000 GW/cm^2 is needed to reach the maximum transmittance. For the graphene layers epitaxially grown on SiC substrate, the SiC nonlinear absorption signals will dominate in the Z-scans above 200 GW/cm^2 at 1.55 eV. The damage threshold of graphene is determined to be higher than 300 GW/cm^2.

For applications as a saturable absorber, the saturation intensity (I_s) is another crucial parameter [24]. The attenuation of the incident light through a single graphene layer can be described by:

$$I_T - I_{in} = -\frac{\alpha_0}{1 + I_{in} / I_s} \cdot I_{in} \tag{15}$$

where I_{in} is the input light intensity, I_T is the transmitted light intensity, α_0 is the linear absorption coefficient of a single layer of graphene, I_s is the saturation intensity of a single layer of graphene. Considering that light sequentially passes through the different graphene layers, the z position dependent transmittance is calculated from the ratio of the energy of the transmitted pulse to that of the incident pulse. These energies are obtained by integrating I_T and I_{in} (for a Gaussian pulse) over the temporal and spatial domains. Figure 6(a) shows a typical experimental data fitted with I_s as the only unknown parameter. Figure 6(b) shows the obtained saturation intensities vs. pump intensities. The saturation intensity was found to be ~4(± 1) GW/cm^2 for a single layer of graphene and it is independent of the pump intensity.

#122085 - $15.00 USD Received 4 Jan 2010; revised 9 Feb 2010; accepted 9 Feb 2010; published 19 Feb 2010

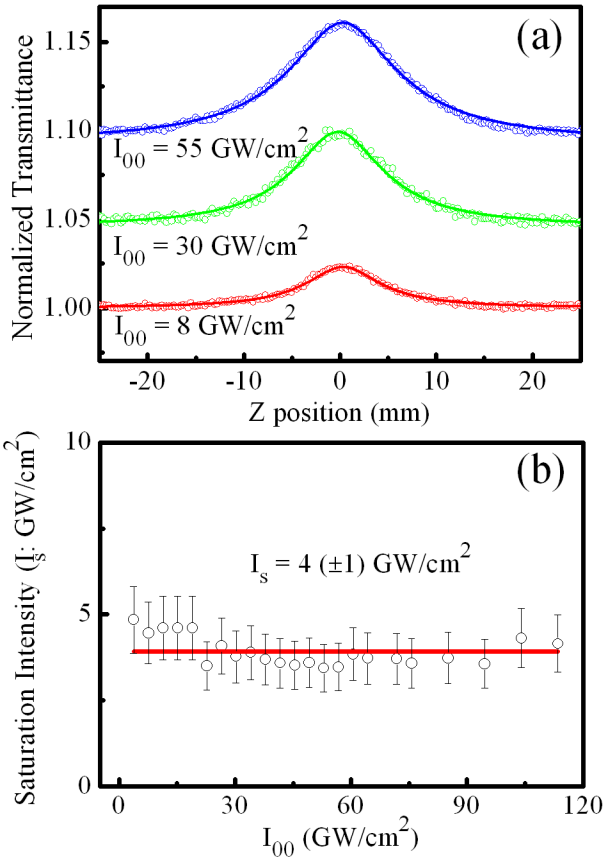

Fig. 6. (a) Typical experimental dates (circle data) fitted with empirical Eq. (14), (b) The obtained I_s vs. pump intensity.

4. Conclusion

The ultrafast saturable absorption properties of graphene is experimentally characterized and theoretically modeled in the femtosecond time regime. The saturable absorption properties of graphene are well-modeled with valence band depletion, conduction band filling and ultrafast intraband carrier thermalization. The ultrafast intraband carrier thermalization is dominated by intraband c-c scattering. With our method of *z*-scan measurements in conjunction with theoretical calculations, the scattering time is determined to be 8 (± 3) fs. Such ultrafast c-c dynamics is far beyond the time resolution of other ultrafast techniques with typical hundred fs laser pulses. In addition, our results show that the spatiotemporal profiles of an intense Gaussian pulse narrow upon transmission through graphene. This narrowing can be controlled either by tuning the incident light intensity or by varying the number of layers. Our findings reveal that graphene possesses great potential for applications as passive mode-lockers, optical pulse shapers or output couplers. Graphene, with all its fascinating properties, continues to offer us new insights into the field of nonlinear optics and their applications.

Acknowledgements

This research is supported by a grant from the Academic Research Fund (AcRF) Tier 1 – RG 49/08 (M52110082) and a NTU start-up grant under Grant No. M58110068.

#122085 - $15.00 USD Received 4 Jan 2010; revised 9 Feb 2010; accepted 9 Feb 2010; published 19 Feb 2010